IEEE Access
Multidisciplinary | Rapid Review | Open Access Journal

Received August 10, 2020, accepted August 23, 2020, date of publication August 26, 2020, date of current version September 9, 2020.

Digital Object Identifier 10.1109/ACCESS.2020.3019691

Grid-Forming Control for DFIG Based Wind Farms to Enhance the Stability of LCC-HVDC

YINGZONG JIAO AND HENG NIAN, (Senior Member, IEEE)
College of Electrical Engineering, Zhejiang University, Hangzhou 310027, China

Corresponding author: Heng Nian (nianheng@zju.edu.cn)

This work was supported by the National Natural Science Foundation of China under Grant 51977194.

ABSTRACT This article presents the grid-forming control (GFC) for doubly-fed induction generator (DFIG)-based wind farm to enhance the stability of line-commutated converter (LCC) based high voltage direct current (HVDC) transmission system. GFC is a grid friendly control strategy to build or follow the grid voltage and provide inertia support for power grid. The GFC for DFIG can not only improve the stability of HVDC sending-terminal system, but also reduce the dependence of synchronous generator (SG) in HVDC sending-terminal system. Impedance analysis is used to analyze the stability of HVDC sending-terminal system. The impedance modeling process of the GFC for DFIG is introduced in detail. Based on the impedance analysis, the GFC for DFIG shows the better stability than the conventional vector control (VC) for DFIG in HVDC sending-terminal system. When the capacity of SG decreases and transmission line impedance increases, the GFC for DFIG can keep stable, while the VC for DFIG will lose the stability in HVDC sending-terminal system. Vector graph of impedance characteristic is applied to illustrate the mechanism of instability. The time domain simulations are presented to verify the impedance analysis. Moreover, the simulation in islanded condition is also given to illustrate the stability and effectiveness of the GFC for DFIG.

INDEX TERMS Grid-forming control, line-commutated converter (LCC) based high-voltage direct current (HVDC) transmission, doubly-fed induction generator, impedance modeling.

I. INTRODUCTION

Line-commutated converter (LCC) based high voltage direct current (HVDC) transmission systems have been widely utilized worldwide. With the benefits of the enhanced power controllability, efficient cost and power transmission capability, HVDC is considered to be a suitable scheme for the long-distance transmission of renewable power generations [1], [2], [23], [24].

The doubly-fed induction generator (DFIG) based wind farms have been widely installed in the renewable power generation system [3], [4]. However, as the penetration of wind farms increases rapidly, the instability and faults in the power system may become more frequent and severe, such as the big shutdown of Great Britain power grid in 2019 [5]. According to the event report, the low level inertia characteristic of wind generation is the main reason of the shutdown. The conventional control strategy of DFIG is the vector control (VC), which follows the grid voltage and does not provide the inertia and voltage support during grid faults. Therefore, 'grid-forming control' (GFC), which can help renewable power generations to improve the inertia of power system, is attracting a wide-spread attention.

GFC is a grid-friendly control method, which emulates the working principle of synchronous generators (SG). In GFC, the swing equation of SG is used to build or follow the grid voltage and control active power [6], [7]. According to [6], the GFC inherits the advantages of SGs, which can provide inertia support for power system. In [8], [9], "virtual synchronized control" for DFIG is presented to increase the inertia support capability and improve the frequency stability of weak grid. Furthermore, the GFC control shows the superior small-signal stability better than conventional VC when DFIG is connected to weak grid [10], [11].

In HVDC sending-terminal system, there are usually SGs or static-synchronous-compensator (STATCOM) to provide the voltage and frequency support [12], [13], which increases the cost of HVDC and limit the implementation of HVDC

The associate editor coordinating the review of this manuscript and approving it for publication was Guangdeng Zong.

in offshore condition. Synchronverter-based control strategy for voltage source converters (VSC) based HVDC system has been presented in [14]. However, due to the limited control capability of LCC-HVDC, the GFC cannot be implemented in LCC-HVDC transmission system. Therefore, the GFC for DFIG is a considerable technology route, when offshore wind farms connect to the LCC-HVDC sending-terminal. With the GFC control, DFIG based wind farms can build the grid voltage and the SGs or STATCOM can be avoided. The GFC control method can apply to not only the grid-connecting mode but also the islanded mode. Moreover, with the superior small-signal stability of GFC, the stability of HVDC sending-terminal system can be improved.

This article presents the GFC for DFIG-based wind farm with connecting LCC-HVDC and analyzes the stability of HVDC sending-terminal system. The impedance model of the GFC for DFIG is introduced in detail. Then, based on the impedance analysis, the conclusion can be obtained that the GFC for DFIG shows the better stability than the VC for DFIG in HVDC sending-terminal system. Then, the time domain simulations are presented to verify the impedance analysis. Moreover, the simulation in islanded condition is also given to illustrate the stability and effectiveness of the GFC for DFIG.

The contributions of this manuscript can be concluded as: 1) presenting the GFC for DFIG to improve the stability of HVDC sending-terminal system, and building the impedance model of the GFC for DFIG; 2) based on the impedance model, analyzing the stability of HVDC system with considering the capacity and transmission line of SG; 3) the GFC for DFIG can be applied to both grid-connecting mode and islanded mode, it can not only build and support grid voltage, but decrease the dependence on the SG.

The rest of this article is organized as follows. In section II, the GFC for DFIG are introduced, then, the impedance modeling process of GFC for DFIG is presented in detail, the impedance characteristics of VC for DFIG, SG and HVDC sending-terminal are also analyzed. In section III, based on the impedance model, the stability of HVDC sending-terminal system are analyzed with consideration of the capacity and transmission line of SG, and the vector graph of impedance is presented to illustrate the mechanism of instability. In section IV, time domain simulation studies are implemented to verify the stability and effectiveness of the GFC for DFIG in both grid-connecting mode and islanded mode. Finally, the conclusion is drawn in section V.

II. DESCRIPTION OF STUDY SYSTEM AND IMPEDANCE MODELING

Firstly, the case system and the GFC control of DFIG are introduced in this section. Then, the impedance modeling process of DFIG system under GFC control is presented in detail, and the impedance curves of VC control for DFIG, SG and HVDC sending-terminal are also given in this section. Finally, the characteristics of impedance model among the DFIG, SG and HVDC sending-terminal are analyzed, and the potential unstable phenomenon of HVDC sending-system are also presented. The detailed analysis based on the impedance model will be illustrated in the next section.

A. BRIEF DESCRIPTION OF STUDY SYSTEM

The study system is shown in the Fig. 1, where the wind farm, the SG and the HVDC sending-terminal are connected to the AC-grid directly at the point of common coupling (PCC). In Fig. 1, the wind farm consists of DFIG system, where the rotor side converter (RSC) of DFIG is controlled with GFC or VC and the grid side converter (GSC) is controlled with conventional VC [15]. The conventional SG power plant is connected to the PCC with an AC transmission line, while the LCC-HVDC sending-terminal system includes the HVDC rectifier, AC filter and DC cable, the HVDC rectifier works under constant DC current control mode in this manuscript. The parameters of study system are given in the APPENDIX.B.

B. GFC CONTROL FOR DFIG AND IMPEDANCE MODELING

The grid-forming control for DFIG is presented in the Fig. 2. The key of GFC is to control the magnitude and phase of internal voltage. The air gap flux can be defined to represent the internal voltage $\boldsymbol{E}^*_{DFIG}$ in DFIG. The phase of internal voltage can be controlled by swing equation and active power control, and the magnitude of internal voltage can be calculated by reactive power control. The detailed illustration of GFC for DFIG can be referred in [16].

According to the Fig.2, the impedance model of GFC for DFIG includes four parts, i.e., DFIG model, feedback calculation, GFC control loops and frame transformation. The impedance modeling process will be presented in the following. For clarity, bold letters are used in this manuscript to denote complex space vectors, e.g., $\boldsymbol{X} = Xd + jXq$, and bold letters also denote complex transfer functions or transfer matrices, e.g., $\boldsymbol{X}(s) = Xd(s) + jXq(s)$. Impedance modeling bases on the small signal analysis [17], therefore, the state variables with a small-signal perturbation can be written as:

$$x = X_0 + \Delta x \tag{1}$$

where x is the state variable, X_0 is the steady-state value, Δx is the small-signal perturbation. It should be noted that GSC has little influence on small-signal stability, the analysis of GSC will be neglected in the following [18], [19].

1) DFIG MODEL AND FEEDBACK CALCULATION

The DFIG circuit model is given in the Fig. 3, where $\boldsymbol{U}_s$ and $\boldsymbol{U}_r$ are the stator and rotor voltage respectively, $\boldsymbol{I}_s$ and $\boldsymbol{I}_r$ are the stator and rotor current respectively, ψ_s and ψ_r are the stator and rotor flux respectively, R_s and R_r are the stator and rotor resistance respectively, L_s, L_r and L_m are the stator, rotor and mutual inductance respectively, $L_{s\sigma}$ and $L_{r\sigma}$ are the stator, and rotor leakage inductance respectively, ω and ω_s are the synchronous rotating frame (SRF) and slip angular frequency. Taking the Laplace transformation and the

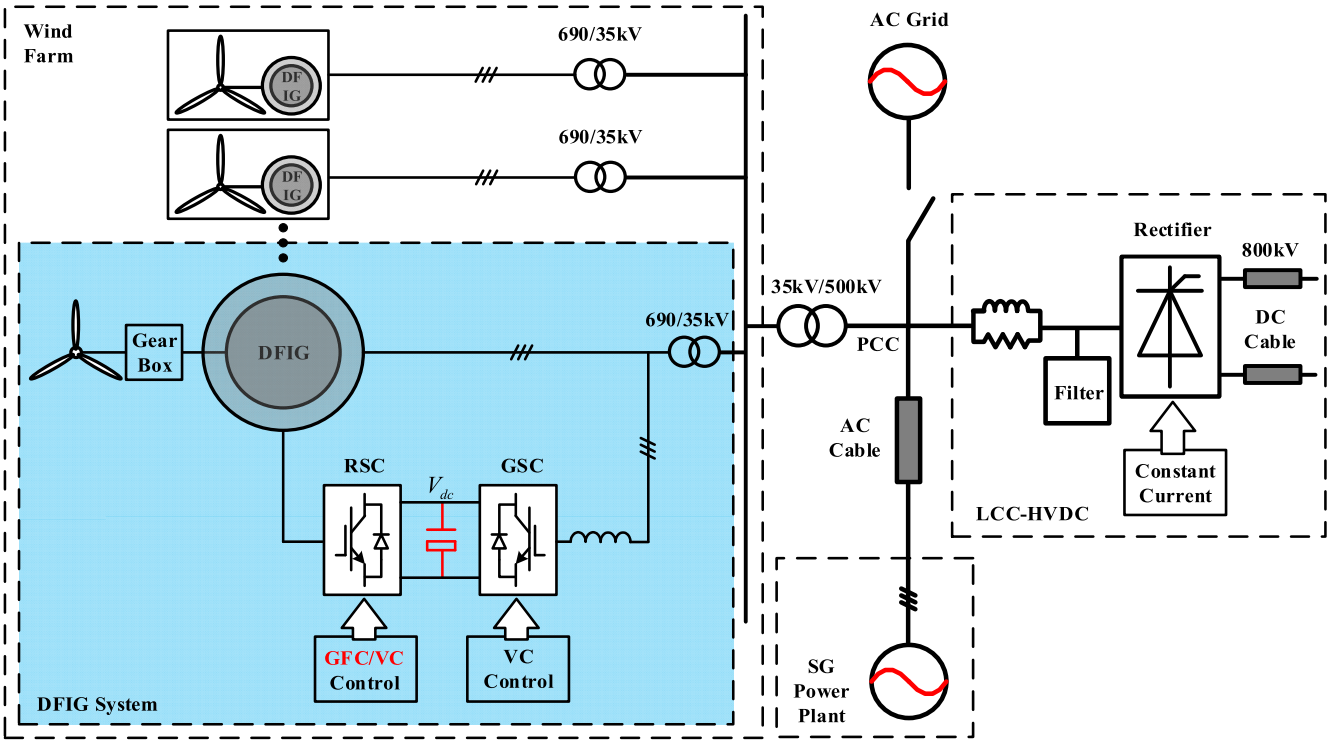

FIGURE 1. The study system.

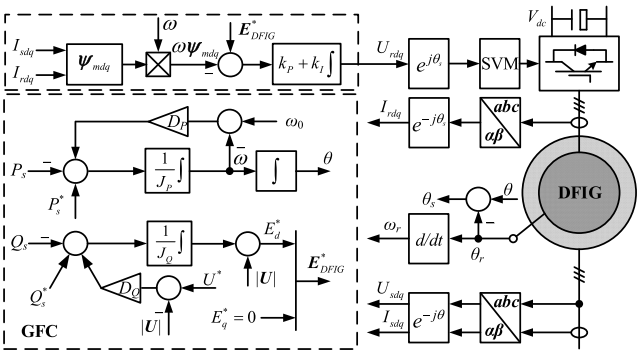

FIGURE 2. Grid-forming control for DFIG.

DFIG model in the SRF can be expressed as:

$$\Delta \boldsymbol{I}_{sdq} = \boldsymbol{G}_{us\_is}(s)\Delta \boldsymbol{U}_{sdq} + \boldsymbol{G}_{ur\_is}(s)\Delta \boldsymbol{U}_{rdq} \quad (2)$$

$$\Delta \boldsymbol{I}_{rdq} = \boldsymbol{G}_{us\_ir}(s)\Delta \boldsymbol{U}_{sdq} + \boldsymbol{G}_{ur\_ir}(s)\Delta \boldsymbol{U}_{rdq} \quad (3)$$

where $\boldsymbol{G}_{us\_is}(s)$ is the transfer matrix from stator voltage to stator current. For simplicity, '(s)'will be neglected in the following expression.

The small-signal-model of active and reactive power can be expressed as:

$$\begin{cases} \begin{bmatrix} \Delta P_s \\ 0 \end{bmatrix} = \boldsymbol{G}_{is\_Ps}\Delta \boldsymbol{I}_{sdq} + \boldsymbol{G}_{us\_Ps}\Delta \boldsymbol{U}_{sdq} \\ \begin{bmatrix} \Delta Q_s \\ 0 \end{bmatrix} = \boldsymbol{G}_{is\_Qs}\Delta \boldsymbol{I}_{sdq} + \boldsymbol{G}_{us\_Qs}\Delta \boldsymbol{U}_{sdq} \end{cases} \quad (4)$$

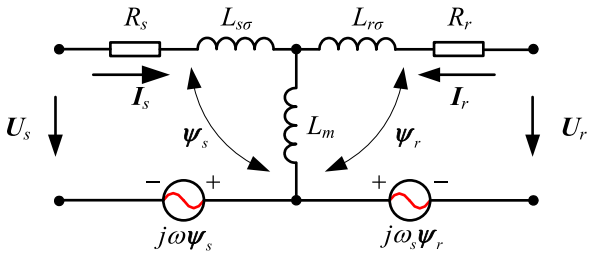

FIGURE 3. Equivalent circuit of DFIG model.

where P_s and Q_s are the active and reactive power of stator respectively.

The small signal model of stator voltage amplitude calculation can be expressed as:

$$\begin{bmatrix} \Delta|\boldsymbol{U}| \\ 0 \end{bmatrix} = \overbrace{\frac{1}{U_0}\begin{bmatrix} u_{sd0} & u_{sq0} \\ 0 & 0 \end{bmatrix}}^{\boldsymbol{G}_U} \begin{bmatrix} \Delta u_{sd} \\ \Delta u_{sq} \end{bmatrix} \quad (5)$$

where Δu_{sd} and Δu_{sq} are the small signal of stator voltage in d-q axis, $|\boldsymbol{U}|$ is the magnitude of stator voltage, U_0 is the rated stator voltage, and $\boldsymbol{G}_U$ is the transfer function from stator voltage to voltage magnitude.

2) MODELING OF GRID-FORMING CONTROL FOR DFIG

The small-signal-model of swing equation can be expressed as:

$$\begin{aligned} \begin{bmatrix} \Delta\theta \\ 0 \end{bmatrix} &= \boldsymbol{G}_{Ps\_\theta}\Delta P \\ &= \boldsymbol{G}_{Ps\_\theta}\boldsymbol{G}_{is\_Ps}\Delta \boldsymbol{I}_{sdq} + \boldsymbol{G}_{Ps\_\theta}\boldsymbol{G}_{us\_Ps}\Delta \boldsymbol{U}_{sdq} \end{aligned} \quad (6)$$

where θ is the virtual synchronous angular, it can be used in virtual synchronous rotating frame (VSRF) transformation in GFC.

The small signal model of reactive power control loop can be expressed as:

$$\begin{aligned}\begin{bmatrix}\Delta E_d^* \\ 0\end{bmatrix} &= \boldsymbol{G}_{Qs\_E}\begin{bmatrix}\Delta Q_s \\ 0\end{bmatrix} + \boldsymbol{G}_{Us\_E}\begin{bmatrix}\Delta|\boldsymbol{U}| \\ 0\end{bmatrix} \\ &= \boldsymbol{G}_{Qs\_E}\boldsymbol{G}_{is\_Qs}\Delta\boldsymbol{I}_{sdq} + \boldsymbol{G}_{Qs\_E}\boldsymbol{G}_{us\_Qs}\Delta\boldsymbol{U}_{sdq} \\ &\quad + \boldsymbol{G}_{U\_E}\boldsymbol{G}_U\Delta\boldsymbol{U}_{sdq} \end{aligned} \tag{7}$$

where $\boldsymbol{E}*d$ is the internal voltage reference in the d-axis of VSRF.

Based on the (6)-(7), the phase and magnitude of internal voltage $\boldsymbol{E}^*_{DFIG}$ of GFC can be obtained, then the rotor voltage can be used to control the feedback of $\boldsymbol{E}^*_{DFIG}$. The small-signal-model of rotor voltage control loop can be expressed as:

$$\begin{aligned}\Delta\boldsymbol{U}_{rdq}^{VSRF} &= \boldsymbol{G}_{PI}(\Delta\boldsymbol{E}^*_{DFIG} - \Delta\boldsymbol{\psi}_{mdq}^{VSRF}) \\ &= \boldsymbol{G}_{PI}(\Delta\boldsymbol{E}^*_{DFIG} - (\omega L_m\Delta\boldsymbol{I}_{sdq}^{VSRF} + \omega L_m\Delta\boldsymbol{I}_{rdq}^{VSRF})) \end{aligned} \tag{8}$$

where the superscript 'VSRF' means the variables in the VSRF, $\boldsymbol{G}_{PI}$ is the transfer matrix of air gap flux ψ_{mdq} controller.

3) MODELING OF FRAME TRANSFORMATION

Because of the dynamics of swing equation, there is an angular perturbation in the frame transformation from SRF to VSRF [17]. The small-signal-model of frame transformation can be expressed as:

$$\begin{aligned}\boldsymbol{X}_{dq}^{VSRF} &= \boldsymbol{X}e^{-j\theta} \approx (\boldsymbol{X}_{dq} + \Delta\boldsymbol{X}_{dq})(1 - j\Delta\theta) \\ &= \boldsymbol{X}_{dq} + \Delta\boldsymbol{X}_{dq} - j\boldsymbol{X}_{dq}\Delta\theta \Rightarrow \Delta\boldsymbol{X}_{dq}^{VSRF} \\ &= \Delta\boldsymbol{X}_{dq} - j\boldsymbol{X}_{dq}\Delta\theta \end{aligned} \tag{9}$$

where $\boldsymbol{X}$ denotes the rotor voltage, stator current and rotor current in (8).

4) IMPEDANCE MODEL OF GFC CONTROL FOR DFIG AND VALIDATION

Based on (2)-(9), the dq-domain impedance model of GFC control for DFIG can be obtained in the SRF, A general dq-frame impedance matrix $\boldsymbol{Z}_{dq}(s)$ is expressed as:

$$\boldsymbol{Z}_{dq}(s) = \begin{bmatrix} Z_{dd}(s) & Z_{dq}(s) \\ Z_{qd}(s) & Z_{qq}(s)\end{bmatrix} \tag{10}$$

The detailed expression of (2)-(10) can be found in the APPENDIX.A. In the unified impedance theory [17], the positive sequence component of impedance model can be expressed as:

$$\boldsymbol{Z}^+_{GFC}(s) = \frac{Z_{dd}(s) + Z_{qq}(s)}{2} + j\frac{Z_{qd}(s) - Z_{dq}(s)}{2} \tag{11}$$

Fig. 4 shows the impedance result of GFC for DFIG in bode diagram, where the black curve is the result of impedance

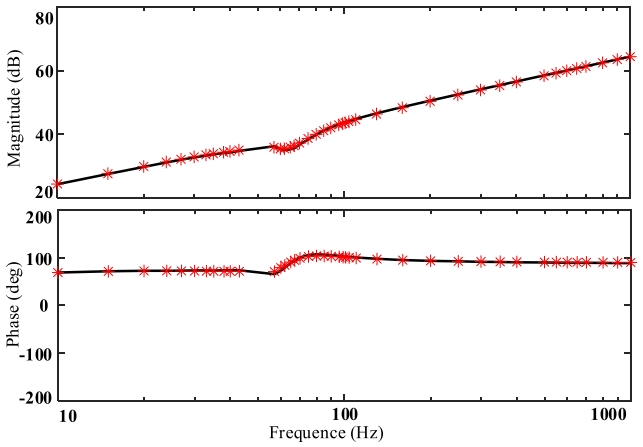

FIGURE 4. Impedance of GFC for DFIG in bode diagram.

model, and the red asterisk is the frequency scanning results obtained from simulation. The frequency scanning results match the model curve well, which validates the correctness of impedance model. It can be found that the impedance of GFC for DFIG has the characteristics of inductance and resistance in the whole frequency range, which is similar to the characteristic of SG.

C. IMPEDANCE MODEL OF VC FOR DFIG, SG AND HVDC

The impedance model of VC for DFIG has been analyzed in [20], the impedance model of SG can also be similarly obtained. For the limited length of paper, the detailed impedance expressions are omitted. The impedance of HVDC sending-terminal system (including AC filters) can be obtained based on frequency scanning method [21], [22].

Fig. 5 presents the impedance results in bode diagram, where the blue curve is the result of VC for DFIG, the red curve is the result of SG, while the black curve is the result of HVDC sending-terminal. The impedance of VC for DFIG

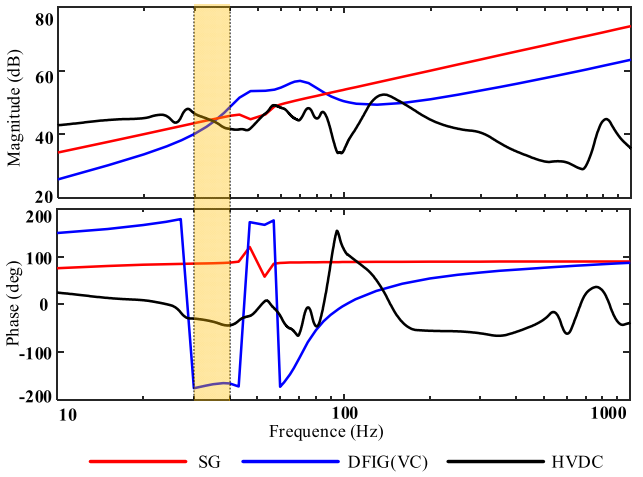

FIGURE 5. Impedance model of VC for DFIG (blue curves), SG (red curves) AND HVDC Sending-Terminal (black curves).

shows the characteristic of negative resistance in the low frequency range, especially in sub-synchronous frequency range. The impedance of SG has the characteristics of resistance and inductance in whole frequency range. And the impedance of HVDC sending-terminal shows the characteristics of capacitance and resistance in the most frequency range.

According to the impedance theory [17], the instability occurs at the frequency where the magnitude curves intersect and phase difference exceeds 180°. As the magnitude of SG impedance changes, there will be an intersection on the three magnitude curves. Therefore, in the Fig. 5, the yellow zone is a potential instability frequency range, since the VC for DFIG, SG and HVDC sending-terminal show the characteristics of negative resistance, inductance and capacitance, respectively. The impedance of GFC for DFIG only has the characteristics of inductance and resistance, which ensures the phase difference less than 180°. Compared with VC for DFIG, the GFC for DFIG shows the better stability in HVDC sending-terminal system. The detailed quantitative analysis based on impedance model will be presented in the section III.

III. STABILITY ANALYSIS

In this section, stability analysis of HVDC sending-terminal system will be presented based on impedance model. According to the analysis in section II. C, there is a potential instability due to the negative resistance impedance characteristic of VC for DFIG. And the increasing of magnitude of SG may induce the instability. When the voltage level keeps constant, the smaller capacity of SG is, the impedance magnitude will be bigger. Moreover, as the length of transmission line increases, the magnitude of line impedance also increases. The impedance of transmission line connecting to SG can be represented by short circuit ratio (SCR). Therefore, the capacity of SG and the SCR on the stability of HVDC sending-terminal system will be analyzed in the following.

To illustrate the mechanism of instability more intuitively, the parallel equivalent impedance of DFIG based wind farm and SG can be defined as:

$$\begin{aligned} \boldsymbol{Z}^{+}_{PLANT}(s) &= \boldsymbol{Z}^{+}_{DFIG}(s) \,//\, \boldsymbol{Z}^{+}_{SG}(s) \\ &= \frac{\boldsymbol{Z}^{+}_{DFIG}(s) \times \boldsymbol{Z}^{+}_{SG}(s)}{\boldsymbol{Z}^{+}_{DFIG}(s) + \boldsymbol{Z}^{+}_{SG}(s)} \end{aligned} \tag{12}$$

where $\boldsymbol{Z}^{+}_{PLANT}$ is the parallel equivalent impedance of DFIG wind farm and SG, $\boldsymbol{Z}^{+}_{DFIG}$ is the impedance of DFIG (under GFC or VC), and $\boldsymbol{Z}^{+}_{SG}$ is the impedance of SG.

The vector graph of impedance will be presented to analyze the difference of impedance characteristics between grid-forming control and vector control from physical view.

A. INFLUENCE OF THE CAPACITY OF SG

Fig. 6 (a)-(c) presents the impedance of GFC for DFIG (blue curves), HVDC sending-terminal (black curves), SG (red curves) and its parallel equivalent impedance (red dashed curves). Fig.6 (a), (b) and (c) show the impedance characteristics of SG with capacity of 500 MW, 200 MW and 100 MW, respectively.

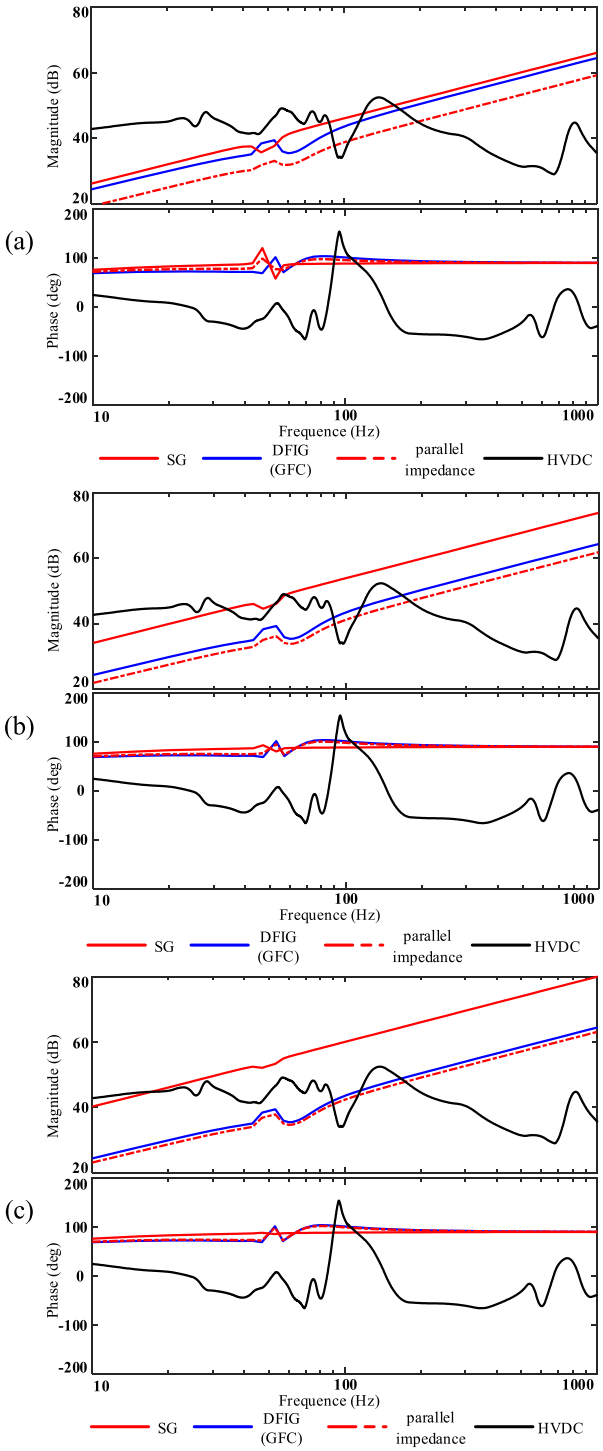

FIGURE 6. Impedance of GFC for DFIG (blue curves), HVDC sending-terminal (black curves), SG (red curves) and its parallel equivalent impedance (red dashed lines). (a) SG is 500MW; (b) SG is 200MW; (C) SG is 100MW.

In the Fig. 6, as the capacity of SG decreases, the magnitude of SG impedance is bigger. However, due to the characteristics of small magnitude of GFC for DFIG, the parallel equivalent impedance with different capacity

of SG are mainly determined by the GFC for DFIG. And the phase curves of parallel equivalent impedance are also mainly determined by the GFC for DFIG, which shows the characteristic of inductance and resistance. According to the fig. 6, the magnitude curves intersections between HVDC sending-terminal and parallel equivalent impedance are located at super-synchronous frequency range, in which the phase difference is less than 180°. GFC for DFIG can ensure the stability in HVDC sending-terminal system considering with different capacity of SG.

With the smaller capacity of SG, the impedance of SG increases, and even to the infinity. According to (12), when impedance of SG is infinity, the parallel equivalent impedance is approximately equal to $\boldsymbol{Z}^{+}_{DFIG}$. In Fig.6, there is no instability intersection between the GFC for DFIG and the HVDC sending-terminal system. It can be concluded that the GFC for DFIG can keep stable in HVDC sending-terminal system, even without SG.

Fig. 7 (a)-(c) presents the impedance results of VC for DFIG (blue curves), the meanings of other curves are the same as the Fig. 6. In the Fig. 7, as the capacity of SG decreases, the magnitude of SG impedance increases, and even exceeds the magnitude of VC for DFIG. When the capacity of SG reduces to 200MW (Fig. 7b), the magnitude of SG impedance will exceed the VC for DFIG, and the parallel impedance will be mainly determined by the VC for DFIG. The phase curves of parallel equivalent impedance mainly show the characteristic of negative resistance and inductance in the sub-synchronous frequency range.

It can be seen from the Fig. 7b that, when the capacity of SG is 200MW, there will be an intersection between HVDC sending-terminal and parallel equivalent impedance locating at the sub-synchronous frequency (38Hz), where the phase difference is more than 180°. According to the impedance theory and analysis above, when the capacity of SG decreases, the VC for DFIG leads to instability in the HVDC sending-terminal system.

To illustrate the mechanism of instability more intuitively, Fig. 8 presents the vector graph of impedance at the instability frequency to understand from physical view. In the Fig. 8(a), all impedance vectors locate at the right half plane, which means that the phase difference is less than 180°, and the GFC for DFIG can ensure the stability of the system. In the Fig. 8(b), because the impedance of VC for DFIG has the characteristic of negative resistance, which leads to the parallel equivalent impedance of DFIG and SG locates at the left half plane and has the characteristic of negative resistance and inductance. The parallel equivalent impedance under the VC for DFIG is on the opposite direction of HVDC sending-terminal. When the capacity of SG decreases, in other words the magnitude of impedance of SG increases, the instability will happen.

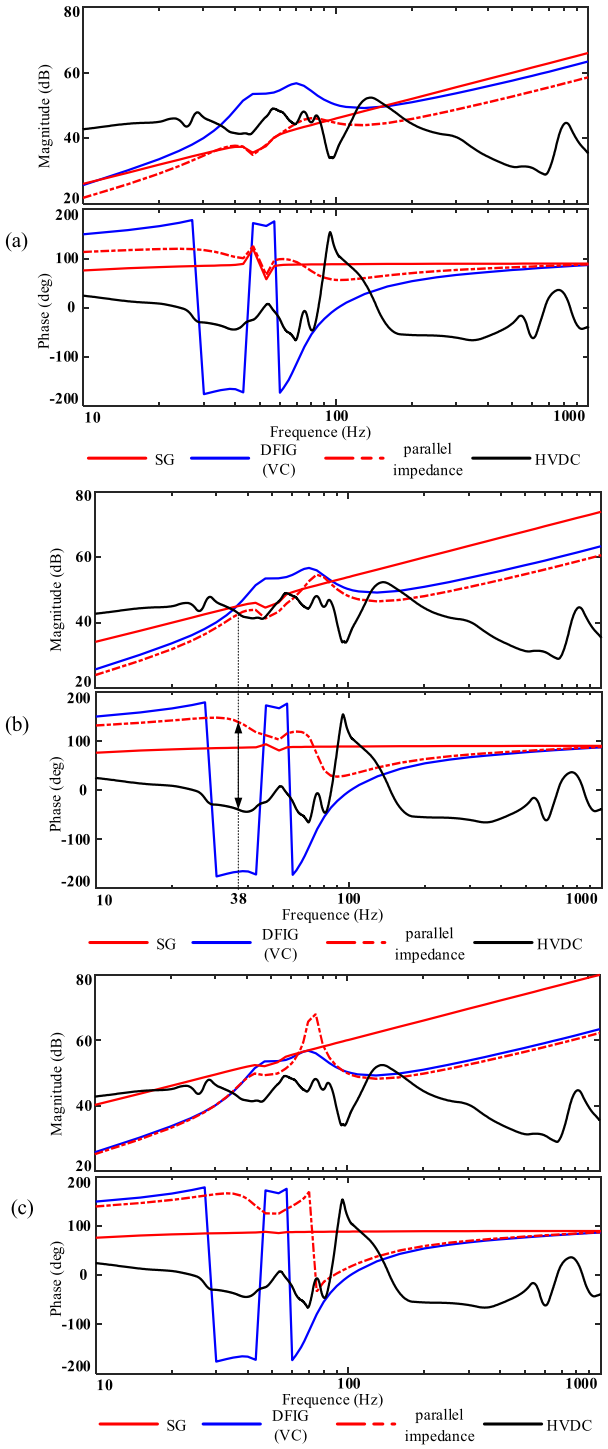

FIGURE 7. Impedance of VC for DFIG (blue curves), HVDC sending-terminal (black curves), SG (red curves) and its parallel equivalent impedance (red dashed). (a) SG 500MW; (b) SG 200MW; (C) SG 100MW.

B. INFLUENCE OF THE CAPACITY OF SCR

Fig. 9 (a)-(c) presents the impedance of GFC for DFIG (blue curves), HVDC sending-terminal (black curves), SG with different SCR (red curves) and its parallel equivalent impedance (red dashed lines). Fig.9 (a), (b) and (c) show the impedance of SG with SCR of 5, 3 and 2, respectively.

Similar with the Fig. 7, though the SCR decreases and the impedance magnitude of SG with transmission line are bigger, the parallel equivalent impedance is determined by

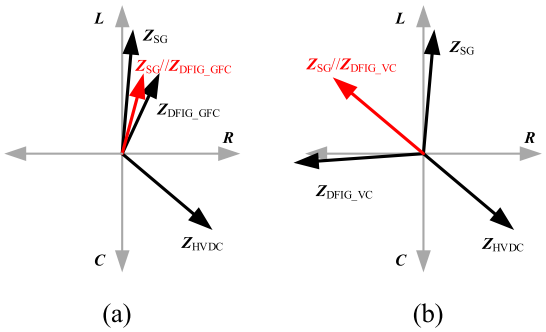

FIGURE 8. Vector graph of impedance (200MW SG) at 38Hz.

the GFC for DFIG. In the Fig. 9, the parallel equivalent impedance has the characteristic of inductance and resistance in the whole frequency range. The characteristic of impedance of GFC for DFIG ensures the stability of HVDC sending-terminal system, considering with different SCR.

Fig. 10 presents the impedance results of VC for DFIG (blue curves), the meanings of other curves are the same as the Fig. 9. In the Fig. 10, as the SCR decreases, the impedance magnitude of SG with transmission line increases, and exceeds the magnitude curve of VC for DFIG in sub-synchronous frequency range. The parallel equivalent impedance mainly shows the characteristic of negative resistance and inductance in the sub-synchronous frequency range. According to the impedance theory, when the SCR decreases, the instability will occur in the HVDC sending-terminal system. The mechanism of instability is similar with the Fig. 8, since the impedance of VC for DIFG has the characteristic of negative resistance.

Based on the analysis above, the following conclusions can be obtained:

1) As the capacity of SG decreases or the SCR decreases, the impedance magnitude of SG will increase, which may lead to the instability in the HVDC sending terminal within the sub-synchronous frequency range, when DFIG wind farm is controlled under VC.

2) The GFC for DFIG has the characteristic of inductance and resistance, which can ensure the stability in HVDC sending-terminal system, even considering with the changing of SG and SCR.

3) The mechanism of instability in the HVDC sending terminal is the negative resistance characteristic of VC for DFIG. When the impedance of SG increases, the parallel equivalent impedance is determined by the VC for DFIG, which has the characteristic of negative resistance and inductance. According to the impedance theory, the instability will occur in the HVDC sending-terminal system, which has the characteristic of capacitance in sub-synchronous frequency range.

IV. SIMULATION RESULTS

In this section, the simulation results are presented to illustrate the correctness of impedance analysis above. The system and control parameters can be found in the APPENDIX.B.

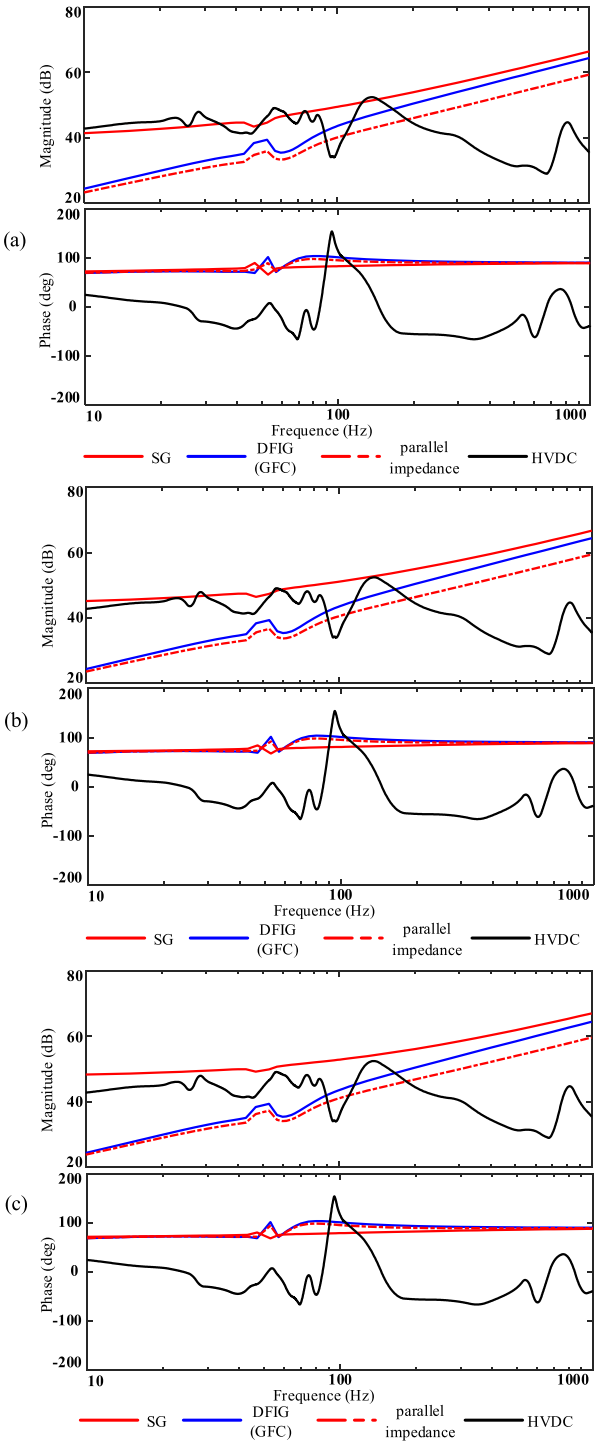

FIGURE 9. Impedance of GFC for DFIG (blue curves), HVDC sending-terminal (black curves), SG (red curves) and its parallel equivalent impedance (red dashed lines). (a) SCR is 5; (b) SCR is 3; (c) SCR is 2.

The rated power of the HVDC and DFIG based wind-farm is 1000MW. The simulations considering with different capacity of SG and different SCR of SG will be given in the following. Moreover, to illustrate the performance of GFC for DFIG, the simulation result of islanded condition without the SG is also presented.

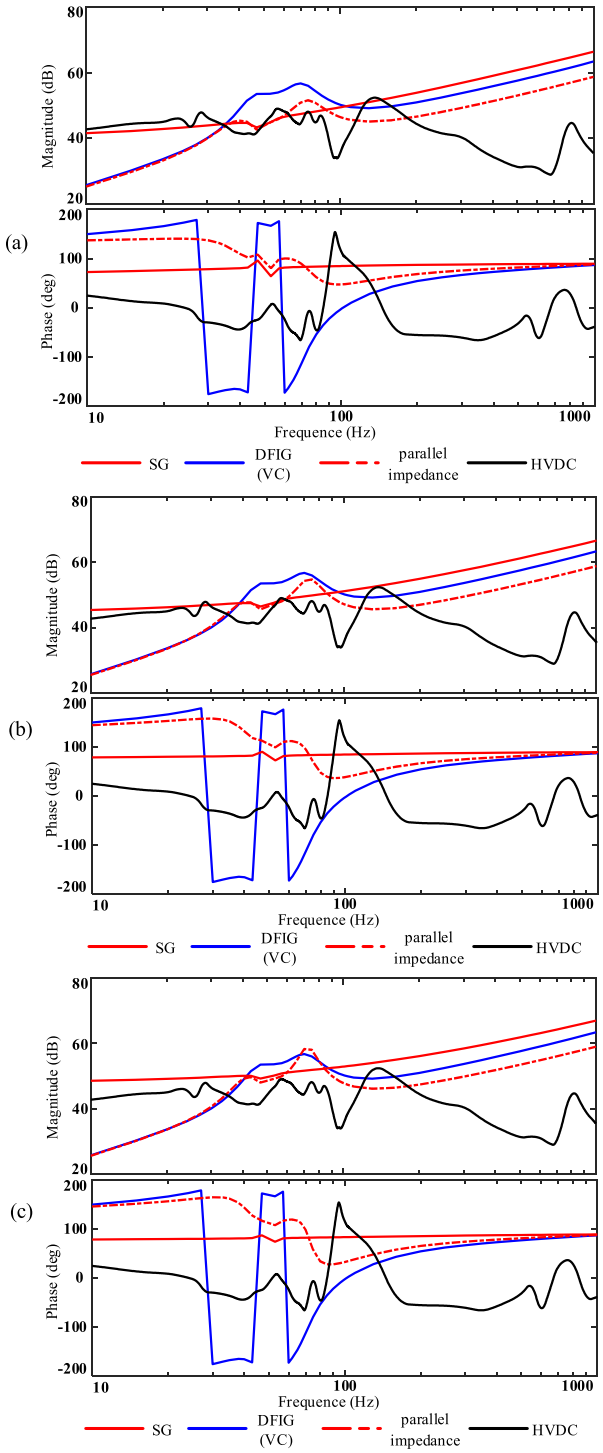

FIGURE 10. Impedance of VC for DFIG (blue curves), HVDC sending-terminal (black curves), SG (red curves) and its parallel equivalent impedance (red dashed lines). (a) SCR is 5; (b) SCR is 3; (c) SCR is 2.

A. SIMULATION RESULTS OF DIFFERENT CAPACITY OF SG

Fig. 11 (a)-(c) presents the simulation results of stator current of DFIG, in which the capacity of SG is 500MW, 200MW, 100MW, respectively. At first, the DFIG is controlled under GFC. Then, at 1s, the control method of DFIG changes from GFC to VC. It can be seen that the GFC for DFIG keeps stable with different capacity of SG. However, as the capacity of SG decreases, the sub-synchronous resonance occurs in the DFIG with VC. In Fig. 11(a), when the capacity of SG is 500MW, the system remains stable. When the capacity of SG below 200MW, a sub-synchronous resonance current occurs. It can be concluded that the small capacity of SG may induce the instability of VC for DFIG in HVDC sending-terminal system, and the GFC for DFIG has the better stability characteristic than VC for DFIG.

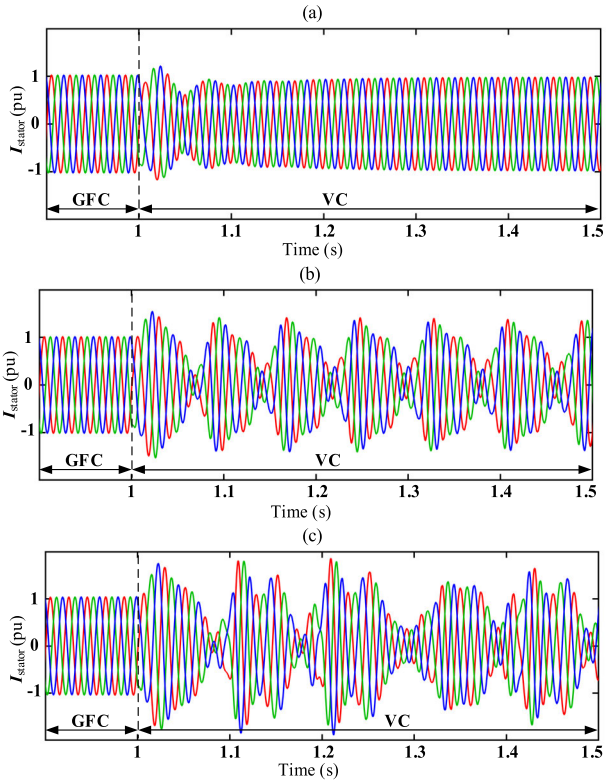

FIGURE 11. Simulation result of stator current with different capacity of SG. (a) SG = 500 MW. (b) SG = 200 MW. (c) SG = 100 MW.

To examine the impedance analysis quantitatively, the fast-Fourier-transform (FFT) result of stator current in Fig. 11(b) is presented in the fig. 12. It can be seen that there is a current resonance at sub-synchronous frequency 38 Hz, which is consistent with the theoretical analysis of impedance model in the Fig. 7(b).

B. SIMULATION RESULTS OF DIFFERENT SHORT CIRCUIT RATIO

Fig. 13 (a)-(c) presents the simulation results of stator current of DFIG with vector control, in which the SCR of SG is 5, 3, 2, respectively. Similarly, at first, the DFIG is controlled under GFC. Then, at 1s, the control method of DFIG changes from GFC to VC. It can be seen that the GFC for DFIG keeps stable with different capacity of SG. By contrast, when DFIG is under vector control, as the SCR of SG decreases, the sub-synchronous resonance occurs in the HVDC sending-terminal system. It can be concluded that the small SCR of SG

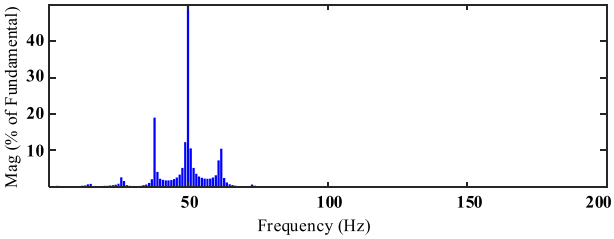

FIGURE 12. FFT result of stator current of VC for DFIG, SG = 200 MW.

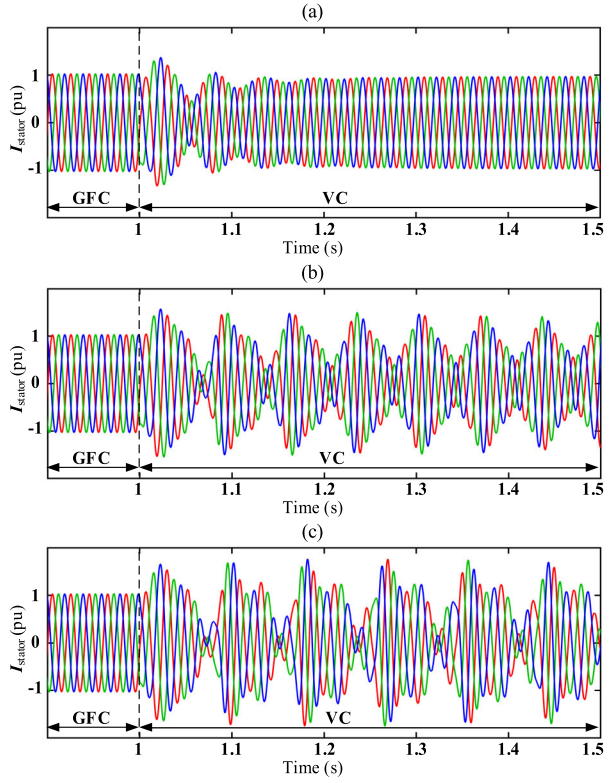

FIGURE 13. Simulation result of stator current with different SCR of SG. (a) SCR = 5. (b) SCR = 3. (c) SCR = 2.

may induce the instability of VC for DFIG in HVDC sending-terminal system, and the GFC for DFIG has the better stability characteristic than VC for DFIG.

C. SIMULATION RESULTS OF GFC FOR DFIG IN ISLANDED CONDITION

To illustrate the performance of GFC for DFIG, the simulation result in islanded condition without the SG is also presented. At 1s, the connection with HVDC sending-terminal system and SG is cut off. Fig. 14 presents the simulation results of stator current of DFIG, stator power of DFIG, AC side current of HVDC rectifier and DC current of HVDC, respectively. It can be seen that the HVDC sending-terminal system keeps stable in both grid-connecting and islanded mode. Though there is a little transient process at 1s, the system returns to the stable condition in 0.2s. The results indicate that the GFC for DFIG can ensure not only the small-signal stability, but the stability of system in different working mode.

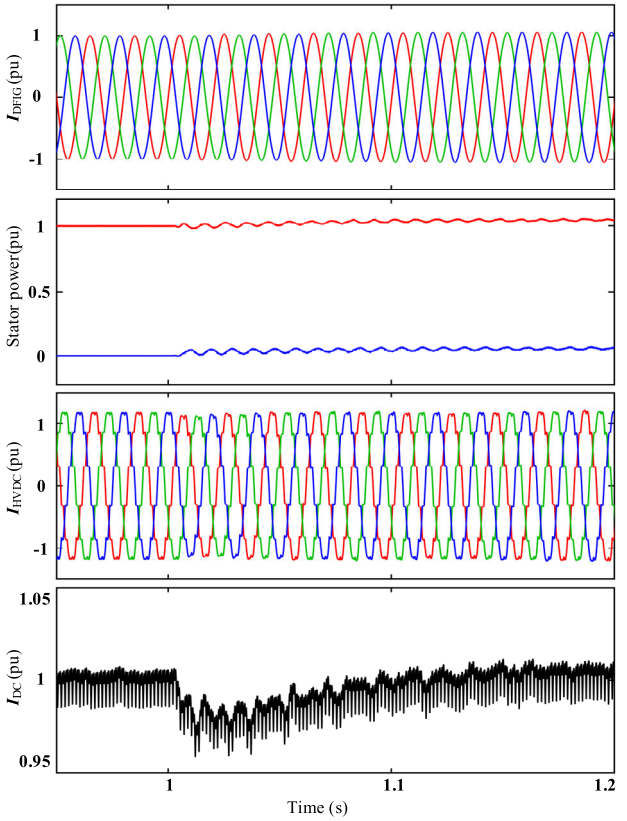

FIGURE 14. Simulation results of DFIG with grid-forming control in islanded condition.

V. CONCLUSION

This article has discussed the grid-forming control for DFIG to enhance the stability of the LCC-HVDC sending-terminal system. The case system including the DFIG with GFC, SG and HVDC sending-terminal is introduced briefly. The impedance modeling process of GFC for DFIG is presented in detail. Based on the impedance model, the stability of HVDC sending-terminal system and the comparison between GFC and VC are analyzed considering with the capacity of SG and SCR. According to the analysis, three conclusions can be obtained: 1) as the capacity of SG decreases or the SCR decreases, it may lead to the instability in sub-synchronous frequency range, when DFIG wind farm is controlled under VC; 2) the GFC for DFIG has the better impedance characteristic than VC for DFIG, the characteristic of GFC for DFIG can ensure the stability in HVDC sending-terminal system, even considering with the changing of SG and SCR; 3) the mechanism of instability is the negative resistance characteristic of VC for DFIG. Time domain simulations are given to validate the correctness of impedance analysis. The GFC for DFIG can ensure not only the small-signal stability, but the stability of HVDC sending-terminal system in both grid-connecting mode and islanded mode.

APPENDIX A
IMPEDANCE MODELING OF GFC

The impedance modeling of DFIG in (2)-(3) can be expressed as:

$$\boldsymbol{G}_1(s) = \begin{bmatrix} R_s + sL_s & -\omega L_s \\ \omega L_s & R_s + sL_s \end{bmatrix} \tag{A1}$$

$$\boldsymbol{G}_2(s) = \begin{bmatrix} sL_m & -\omega L_m \\ \omega L_m & sL_m \end{bmatrix} \tag{A2}$$

$$\boldsymbol{G}_3(s) = \begin{bmatrix} sL_m & -\omega_s L_m \\ \omega_s L_m & sL_m \end{bmatrix} \tag{A3}$$

$$\boldsymbol{G}_4(s) = \begin{bmatrix} R_r + sL_r & -\omega_s L_r \\ \omega_s L_r & R_r + sL_r \end{bmatrix} \tag{A4}$$

$$\begin{cases} \boldsymbol{G}_{us\_is} = \boldsymbol{G}_1^{-1} \\ \boldsymbol{G}_{ir\_is} = -\boldsymbol{G}_1^{-1}\boldsymbol{G}_2 \\ \boldsymbol{G}_{us\_ir} = -(-\boldsymbol{G}_3\boldsymbol{G}_1^{-1}\boldsymbol{G}_2 + \boldsymbol{G}_4)^{-1}\boldsymbol{G}_3\boldsymbol{G}_1^{-1} \\ \boldsymbol{G}_{ur\_ir} = (-\boldsymbol{G}_3\boldsymbol{G}_1^{-1}\boldsymbol{G}_2 + \boldsymbol{G}_4)^{-1} \end{cases} \tag{A5}$$

where the superscript -1 represents inverse matrix, and the subscript *us_is* represents the transfer matrix from stator voltage to stator current, the meanings of other subscripts are similar to this.

The impedance modeling of feedback calculation in (4)-(5) can be expressed as:

$$\begin{cases} \boldsymbol{G}_{i\_P} = \frac{3}{2}\begin{bmatrix} -u_{sd0} & -u_{sq0} \\ 0 & 0 \end{bmatrix} \\ \boldsymbol{G}_{u\_P} = \frac{3}{2}\begin{bmatrix} -i_{sd0} & -i_{sq0} \\ 0 & 0 \end{bmatrix} \\ \boldsymbol{G}_{i\_Q} = \frac{3}{2}\begin{bmatrix} -u_{sq0} & u_{sd0} \\ 0 & 0 \end{bmatrix} \\ \boldsymbol{G}_{u\_Q} = \frac{3}{2}\begin{bmatrix} i_{sq0} & -i_{sd0} \\ 0 & 0 \end{bmatrix} \end{cases} \tag{A6}$$

where u_{sd0} and u_{sq0} are the stator voltage in d-q axis, i_{sd0} and i_{sq0} are the stator current in d-q axis.

The modeling of GFC control loops in (6)-(7) can be expressed as:

$$\boldsymbol{G}_{P\_\theta} = \begin{bmatrix} \frac{1}{s}\frac{-1}{J_P s + D_P} & 0 \\ 0 & 0 \end{bmatrix} \tag{A7}$$

$$\boldsymbol{G}_{Q\_E} = \begin{bmatrix} \frac{-1}{J_Q s} & 0 \\ 0 & 0 \end{bmatrix} \tag{A8}$$

$$\boldsymbol{G}_{U\_E} = \begin{bmatrix} -D_Q & 0 \\ 0 & 0 \end{bmatrix} \tag{A9}$$

where J_P and D_P are the inertia and damping in active power control, J_Q and D_Q are the inertia and damping in reactive power control.

TABLE 1. Parameters of HVDC sending terminal system.

Parameter	Value	Parameter	Value
Rated power	1000 MW	Rated AC voltage	500 kV
Rated DC voltage	800 kV	Rated frequency	50 Hz
Integral of PLL	1400 pu	Proportional of PLL	60 pu
Integral of current control	500 pu	Proportional of current control	5 pu
Reactive power of filter 1	150 Mvar	Reactive power of filter 2 (11th)	150 Mvar
Quality factor of filter 2 (11th)	100	Reactive power of filter 3 (13th)	150 Mvar
Quality factor of filter 3 (13th)	100	Reactive power of filter 4 (24th)	150 Mvar
Quality factor of filter 4 (24th)	3	Resistance of parallel filter	26.07 Ω
Inductance of parallel filter	48.86 mH	DC current inductance	1 H

TABLE 2. Parameters of DFIG based wind farm.

Parameter	Value	Parameter	Value
Rated power	2 MW	Rated AC voltage	690 V
Rated DC voltage	1200 V	Rated frequency	50 Hz
Stator resistance	0.0127 pu	Rotor resistance	0.0127 pu
Stator inductance	0.171 pu	Rotor inductance	0.167 pu
Mutual inductance	3.9 pu	Rotor speed	1.2 pu
Integral of PLL	1400 pu	Proportional of PLL	60 pu
Integral of DC voltage control	50 pu	Proportional of DC control	5 pu
Integral of GSC current control	100 pu	Proportional of GSC control	1 pu
Inertia of active power in GFC	100 pu	Damping of active power in GFC	50 pu
Inertia of reactive power in GFC	1000 pu	Damping of reactive power in GFC	10 pu
Integral of internal voltage control	100 pu	Proportional of internal voltage control	1 pu
Inductance of parallel filter	48.86 mH	DC current inductance	1 H

The modeling of rotor voltage control loop in (8) can be expressed as:

$$\boldsymbol{G}_{PI} = \begin{bmatrix} \frac{1}{2}\frac{k_P s + k_I}{s} & 0 \\ 0 & \frac{1}{2}\frac{k_P s + k_I}{s} \end{bmatrix} \tag{A10}$$

The modeling of frame transformation control loop in (9) can be expressed as:

$$\boldsymbol{G}_{urdq0} = \begin{bmatrix} u_{rq0} & 0 \\ -u_{rd0} & 0 \end{bmatrix} \tag{A11}$$

$$\boldsymbol{G}_{isdq0} = \begin{bmatrix} i_{sq0} & 0 \\ -i_{sd0} & 0 \end{bmatrix} \tag{A12}$$

$$\boldsymbol{G}_{irdq0} = \begin{bmatrix} i_{rq0} & 0 \\ -i_{rd0} & 0 \end{bmatrix} \tag{A13}$$

where u_{rd0} and u_{rq0} are the rotor voltage in d-q axis, $\boldsymbol{G}_{urdq0}$, $\boldsymbol{G}_{isdq0}$ and $\boldsymbol{G}_{irdq0}$ are the transfer matrix from VSRF to SRF.

TABLE 3. Parameters of SG.

Parameter	Value	Parameter	Value
Rated frequency	50 Hz	Rated AC voltage	690 V
Resistance of internal impedance	0.01 pu	Inductance of internal impedance	0.2 pu
Inertia of SG	100000 kg.m^2	Damping factor of SG	50 pu_T/pu_w

Based on impedance theory, the impedance can be defined as:

$$\boldsymbol{U}_{sdq} = -\boldsymbol{Z}_{dq}\boldsymbol{I}_{sdq} \tag{A14}$$

$$\boldsymbol{Z}_{dq} = \frac{\boldsymbol{G}_{ur\_ir}\boldsymbol{G}_{ir\_ur} + \boldsymbol{G}_{ur\_ir}\boldsymbol{G}_{ir\_is}\boldsymbol{G}_{is\_ur} - \mathbf{E}}{\boldsymbol{G}_{us\_is} + \boldsymbol{G}_{us\_ir}\boldsymbol{G}_{ir\_is} + \boldsymbol{G}_{us\_ur}\boldsymbol{G}_{ur\_ir}\boldsymbol{G}_{ir\_is}} \tag{A15}$$

where the $\mathbf{E}$ is identity matrix. $\boldsymbol{Z}_{dq}(s)$ is dq-frame impedance model.

APPENDIX B
PARAMETERS OF SYSTEM

The parameters of HVDC sending terminal system are shown in Table 1.

The parameters of DFIG based wind farm are shown in Table 2.

The parameters of SG are shown in Table 3.

REFERENCES

[1] M. Bahrman and B. Johnson, "The ABCs of HVDC transmission technologies," *IEEE Power Energy Mag.*, vol. 5, no. 2, pp. 32–44, Mar. 2007, doi: 10.1109/MPAE.2007.329194.

[2] T. J. Hammons, V. F. Lescale, K. Uecker, M. Haeusler, D. Retzmann, K. Staschus, and S. Lepy, "State of the art in ultrahigh-voltage transmission," *Proc. IEEE*, vol. 100, no. 2, pp. 360–390, Feb. 2012, doi: 10.1109/JPROC.2011.2152310.

[3] Z. Chen, J. M. Guerrero, and F. Blaabjerg, "A review of the state of the art of power electronics for wind turbines," *IEEE Trans. Power Electron.*, vol. 24, no. 8, pp. 1859–1875, Aug. 2009.

[4] F. Blaabjerg and K. Ma, "Future on power electronics for wind turbine systems," *IEEE J. Emerg. Sel. Topics Power Electron.*, vol. 1, no. 3, pp. 139–152, Sep. 2013.

[5] NationalgridESO. (Aug. 2019). *Interim Report into the Low Frequency Demand Disconnection (LFDD) following Generator Trips and Frequency Excursion*. [Online]. Available: https://www.nationalgrideso.com/document/151081/download

[6] Q.-C. Zhong, P.-L. Nguyen, Z. Ma, and W. Sheng, "Self-synchronized synchronverters: Inverters without a dedicated synchronization unit," *IEEE Trans. Power Electron.*, vol. 29, no. 2, pp. 617–630, Feb. 2014.

[7] J. Alipoor, Y. Miura, and T. Ise, "Power system stabilization using virtual synchronous generator with alternating moment of inertia," *IEEE J. Emerg. Sel. Topics Power Electron.*, vol. 3, no. 2, pp. 451–458, Jun. 2015.

[8] S. D'Arco and J. A. Suul, "Equivalence of virtual synchronous machines and frequency-droops for converter-based MicroGrids," *IEEE Trans. Smart Grid*, vol. 5, no. 1, pp. 394–395, Jan. 2014.

[9] J. Liu, Y. Miura, and T. Ise, "Comparison of dynamic characteristics between virtual synchronous generator and droop control in inverter-based distributed generators," *IEEE Trans. Power Electron.*, vol. 31, no. 5, pp. 3600–3611, May 2016.

[10] S. Wang, J. Hu, and X. Yuan, "Virtual synchronous control for grid-connected DFIG-based wind turbines," *IEEE J. Emerg. Sel. Topics Power Electron.*, vol. 3, no. 4, pp. 932–944, Dec. 2015.

[11] L. Huang, H. Xin, L. Zhang, Z. Wang, K. Wu, and H. Wang, "Synchronization and frequency regulation of DFIG-based wind turbine generators with synchronized control," *IEEE Trans. Energy Convers.*, vol. 32, no. 3, pp. 1251–1262, Sep. 2017.

[12] S. V. Bozhko, R. Blasco-Gimnez, R. Li, J. C. Clare, and G. M. Asher, "Control of offshore DFIG-based wind farm grid with line-commutated HVDC connection," *IEEE Trans. Energy Convers.*, vol. 22, no. 1, pp. 71–78, Mar. 2007, doi: 10.1109/TEC.2006.889544.

[13] R. Li, S. Bozhko, and G. Asher, "Frequency control design for offshore wind farm grid with LCC-HVDC link connection," *IEEE Trans. Power Electron.*, vol. 23, no. 3, pp. 1085–1092, May 2008, doi: 10.1109/TPEL.2008.921193.

[14] R. Aouini, B. Marinescu, K. Ben Kilani, and M. Elleuch, "Synchronverter-based emulation and control of HVDC transmission," *IEEE Trans. Power Syst.*, vol. 31, no. 1, pp. 278–286, Jan. 2016, doi: 10.1109/TPWRS.2015.2389822.

[15] A. Tapia, G. Tapia, J. X. Ostolaza, and J. R. Saenz, "Modeling and control of a wind turbine driven doubly fed induction generator," *IEEE Trans. Energy Convers.*, vol. 18, no. 2, pp. 194–204, Jun. 2003.

[16] H. Nian and Y. Jiao, "Improved virtual synchronous generator control of DFIG to ride-through symmetrical voltage fault," *IEEE Trans. Energy Convers.*, vol. 35, no. 2, pp. 672–683, Jun. 2020, doi: 10.1109/TEC.2019.2954596.

[17] X. Wang, L. Harnefors, and F. Blaabjerg, "Unified impedance model of grid-connected voltage-source converters," *IEEE Trans. Power Electron.*, vol. 33, no. 2, pp. 1775–1787, Feb. 2018.

[18] Z. Miao, "Impedance-Model-Based SSR analysis for type 3 wind generator and series-compensated network," *IEEE Trans. Energy Convers.*, vol. 27, no. 4, pp. 984–991, Dec. 2012.

[19] H. Liu, X. Xie, C. Zhang, Y. Li, H. Liu, and Y. Hu, "Quantitative SSR analysis of series-compensated DFIG-based wind farms using aggregated RLC circuit model," *IEEE Trans. Power Syst.*, vol. 32, no. 1, pp. 474–483, Jan. 2017.

[20] Y. Xu, H. Nian, T. Wang, L. Chen, and T. Zheng, "Frequency coupling characteristic modeling and stability analysis of doubly fed induction generator," *IEEE Trans. Energy Convers.*, vol. 33, no. 3, pp. 1475–1486, Sep. 2018, doi: 10.1109/TEC.2018.2800043.

[21] X. Jiang and A. M. Gole, "A frequency scanning method for the identification of harmonic instabilities in HVDC systems," *IEEE Trans. Power Del.*, vol. 10, no. 4, pp. 1875–1881, Oct. 1995, doi: 10.1109/61.473368.

[22] H. Liu and J. Sun, "Impedance-based stability analysis of VSC-based HVDC systems," in *Proc. IEEE 14th Workshop Control Model. for Power Electron. (COMPEL)*, Salt Lake City, UT, USA, Jun. 2013, pp. 1–8, doi: 10.1109/COMPEL.2013.6626395.

[23] H. Ren, G. Zong, and H. R. Karimi, "Asynchronous finite-time filtering of networked switched systems and its application: An event-driven method," *IEEE Trans. Circuits Syst. I, Reg. Papers*, vol. 66, no. 1, pp. 391–402, Jan. 2019, doi: 10.1109/TCSI.2018.2857771.

[24] T. Jiao, W. X. Zheng, and S. Xu, "Unified stability criteria of random nonlinear time-varying impulsive switched systems," *IEEE Trans. Circuits Syst. I, Reg. Papers*, early access, Apr. 20, 2020, doi: 10.1109/TCSI.2020.2983324.